0.77-V drive voltage electro-optic modulator with bandwidth exceeding 67 GHz

Selim Dogru and Nadir Dagli*

Electrical and Computer Engineering Department, University of California at Santa Barbara, Santa Barbara, California 93106, USA
**Corresponding author: dagli@ece.ucsb.edu*

Received August 12, 2014; accepted September 4, 2014;
posted September 22, 2014 (Doc. ID 220854); published October 15, 2014

A 0.77-V drive voltage (V_π) electro-optic modulator with bandwidth exceeding 67 GHz is described. Modulator is a compound semiconductor device fabricated using substrate removal technology. This allows placement of metal electrodes on both sides of an optical waveguide containing a *p-i-n* diode. Hence ohmic losses are reduced significantly. Electrode gap is essentially the same as *i* layer thickness, which can be kept very uniform and small. Waveguide core also contains a MQW, which improves electro-optic efficiency. Lack of *p* doping in the waveguide and large detuning between MQW absorption peak and operating wavelength keep the propagation loss low. Large size of the waveguide also helps to keep coupling loss low. Modulator is designed as a traveling wave device using the loaded line approach, which is used for velocity matching. Combination of these approaches yields a device with the lowest V_π and widest bandwidth. © 2014 Optical Society of America

OCIS codes: (130.4110) Modulators; (130.3120) Integrated optics devices; (130.5990) Semiconductors; (060.5625) Radio frequency photonics; (230.7020) Traveling-wave devices.
http://dx.doi.org/10.1364/OL.39.006074

Electro-optic modulator is a key component for any electro-optic system including fiber optic transmission, microwave photonics, optical signal processing, and instrumentation. There are several performance targets a modulator should meet. The most important ones are a low V_π, a wide electrical and optical bandwidth and low insertion loss. Meeting these targets requires a conflicting set of design rules, and it is very difficult to meet all of these at the same time. For example very wide bandwidth electro-optic modulators have been realized in different technologies such as $LiNbO_3$ [1], polymer [2] and compound semiconductors [3]. But all these devices have V_π larger than 5 V and consume too much electrical power. It is also very difficult to drive them at high frequencies, and typically a separate modulator driver is needed. This is true even for lower bandwidth, commonly used electro-optic modulators. The modulator driver adds to the power consumption, cost, and complexity. It is possible to make broadband electro-optic modulators with V_π as low as 0.2 V [4], but at the present time wide bandwidth versions of these modulators have not been demonstrated. Therefore, there is a genuine need for modulators with less than 1 V V_π and wide bandwidth. This work describes such a modulator with V_π 0.77 V and bandwidth larger than 67 GHz.

Figure 1 shows the modulator described. It is a traveling-wave electro-optic intensity modulator. Optical structure is a Mach–Zehnder interferometer, which consists of two y-branches and arms made out of single-mode optical waveguides. Waveguides are contained in the epilayer, which exists only as two narrow stripes located within the gaps of the electrode. Figure 2 shows the details of the optical waveguide used in the modulator as well as the fundamental mode pattern. This is also one of the phase modulators used in the Mach–Zehnder interferometer arms. Its core is 0.49 μm thick undoped MQW of 33 nm × 10 nm $In_{0.53}Al_{0.08}Ga_{0.39}As$ quantum wells (QW) and 32 nm × 5 nm $In_{0.52}Al_{0.48}As$ barriers. Room temperature photoluminescence peak of this MQW stack is at 1.37 μm. This is 180 nm away from the operating wavelength of 1.55 μm, hence absorption due to MQW is minimal and not a significant contributor to propagation loss.

MQW core is clad above and below with 1.2-μm-thick InP layers. One of the InP layers is *n* doped to 5×10^{17} cm^{-3} level. The other is undoped. Thin InAlAs layers are the barriers to the first and last QWs. These are thicker than the barriers used in MQW stack and act as etch stop layers during fabrication. The design of the waveguide is such that optical mode is entirely contained within the InP cladding and MQW stack. Epilayer also has p^+ and n^+ $In_{0.53}Ga_{0.47}As$ layers on undoped and *n*-doped InP claddings. Therefore, it contains a *p-i-n* diode formed by p^+ $In_{0.53}Ga_{0.47}As$, undoped InP/MQW stack, and *n* InP/n^+ $In_{0.53}Ga_{0.47}As$. n^+ and p^+ $In_{0.53}Ga_{0.47}As$ layers are also used for low-resistance ohmic contact formation. $In_{0.53}Ga_{0.47}As$ layers and ohmic contacts do not overlap with the optical mode. Furthermore, there is no *p* doping within the waveguide. Hence, the propagation loss is mainly due to scattering from etched sidewalls and free carrier (FC) absorption due to *n* InP. Both of these loss components are low and experimentally measured optical propagation loss is about 2.5–4 dB/cm depending on the waveguide width. Waveguide width mainly affects the loss

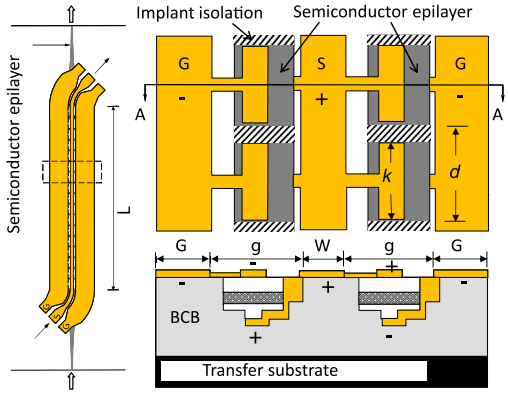

Fig. 1. Top and cross sectional profiles of the modulator.

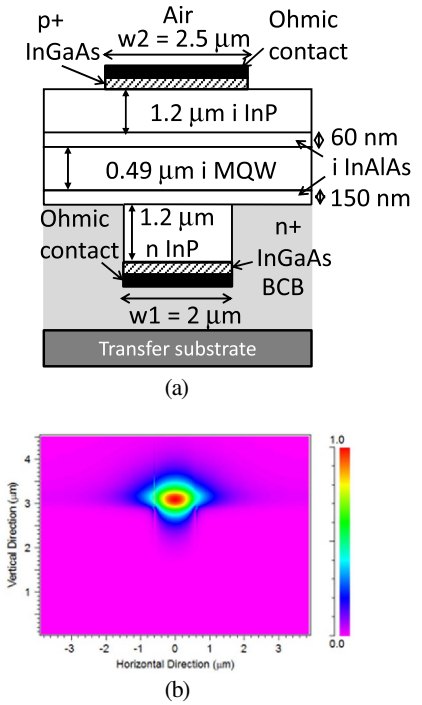

Fig. 2. (a) Cross sectional profile of the optical waveguide used in the modulator. This is also a phase modulator in one of the arms of the Mach–Zehnder interferometer. (b) Optical mode pattern of the fundamental mode.

due to sidewall roughness scattering by changing the mode overlap with etched sidewalls. Width of the waveguides used in the modulator is 2 µm.

Furthermore, big size of the optical mode results in efficient coupling with lensed fibers. Measured coupling loss on waveguides without antireflection (AR)-coated facets is about 3–5 dB per facet depending on waveguide width. Coupling loss can be reduced by about 3 dB per facet by using AR coating and simple mode transformers.

Electrode is a modified coplanar transmission line in ground-signal-ground configuration (G-S-G). Epilayer containing the waveguide is periodically implanted with boron. This implant makes the epilayer highly resistive and breaks the waveguide into sections electrically isolated from one another. Period of this segmentation is d and the length of the ohmic contacts on electrically active epilayer is k. Therefore, only k/d fraction of the optical waveguide contributes to modulation. This ratio is defined as the fill factor.

Ohmic contacts on either side of the epilayer are connected to the coplanar electrode such that the modulating AC voltage, V_{AC}, on the electrode appears across each arm with opposite polarity. This generates push–pull action. Modulator is operated by applying the same reverse bias, V_B to p-i-n diodes in both arms. Due to reversal of the AC voltage polarity, voltage applied to both modulator arms are $V_B + V_{\mathrm{AC}}$ and $V_B - V_{\mathrm{AC}}$. These voltages generate an electric field in the i MQW core and i InP cladding. In this case, thickness of the i-region is essentially the gap of the modulator electrode. This thickness is controlled by crystal growth and can be made very uniform and small. Under reverse bias, a p-i-n diode can be modeled as a capacitor in series with a resistor. Capacitor is due to the capacitance of the i-layer of the p-i-n diode, and resistor is due to the resistance of p and n layers as well as ohmic contacts. The length of short modulating sections, k, is less than 100 µm, which is much less than the microwave wavelength even at 100 GHz. Periodic loading of the regular coplanar line with active modulator sections makes a slow wave electrode, which is actually a filter. There is a Bragg frequency associated with these loading elements. At that frequency, there is a strong back reflection. However, since the period of loading is so small, the Bragg frequency is around several THz. So at least up to 100 GHz loading appear as simple capacitive loading and regular transmission line analysis with increased capacitance per unit length applies. Therefore, each section can be modeled using lumped circuit elements. In this case, the model consists of the series combination of resistance R_p and capacitance ΔC, just described. This results in the electrical equivalent circuit of the electrode shown in Fig. 3.

L_u, C_u, R_u and G_u are inductance, capacitance, resistance and conductance per unit length of the unloaded coplanar line. R_p and ΔC are the resistance and capacitance per unit length of the electrically isolated modulating sections.

Reverse bias and modulating voltage combination across the p-i-n diodes in active modulator sections apply an electric field to the i MQW core and i InP cladding. This creates index changes due to FC depletion, linear and quadratic electro-optic (LEO and QEO) effects. In this case, thickness of the i-region plus the small depletion widths in doped layers is the gap t of the modulator electrode. When a voltage of $V_B \pm V_{\mathrm{AC}}$ is applied to each arm, resulting electric fields are $E_B \pm E_{\mathrm{AC}}$ where $E_B = V_B/t$ and $E_{\mathrm{AC}} = V_{\mathrm{AC}}/t$. The resultant index changes due to FC depletion in the n InP and due to LEO and QEO effects in i InP and MQW can be expressed as:

$$\Delta n_{\mathrm{LEO}} = \frac{1}{2} n_e^3 r_{41} 2\Gamma_{\mathrm{LEO}} E_{\mathrm{AC}},$$

$$\Delta n_{\mathrm{QEO}} = \frac{1}{2} n_e^3 R4 E_B \Gamma_{\mathrm{QEO}} E_{\mathrm{AC}} \quad \text{and}$$

$$\Delta n_{\mathrm{FC}} = 2K_N \Delta N^x \Gamma_N,$$

where n_e is the effective index of the mode, r_{41} is the LEO coefficient, R is the QEO coefficient, Γ_{LEO} and Γ_{QEO} are the overlap factors of the optical mode with the electric fields appropriate for the LEO and QEO effects, Γ_N is the overlap factor of the optical mode with the depleted n InP layer, and K_N and x are the appropriate parameters for n InP. Comparing LEO and QEO index changes, we observe that QEO index change is just like LEO index

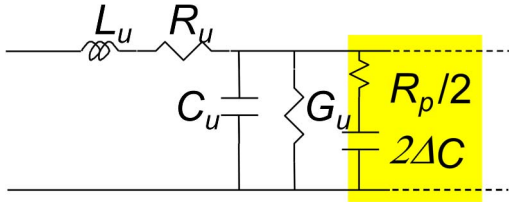

Fig. 3. Electrical equivalent circuit of the modulator electrode.

change with an effective LEO coefficient of $2RE_B$. This is adjustable with E_B and modulation is expected to be more efficient as V_B increases. Using these index changes, we can express V_π i.e., the voltage needed to create a π phase shift between the arms of the interferometer of length L as:

$$V_\pi = \frac{\frac{\lambda}{2L}t - 2K_N\Delta N^x\Gamma_N t}{n_e^3(r_{41}\Gamma_{\mathrm{LEO}} + 2RE_B\Gamma_{\mathrm{QEO}})}.$$

Using $\lambda = 1.55$ μm, $L = 1$ cm, $t = 2.0$ μm, $K_N\Delta N^x = 10^{-3}$ for $N = 10^{17}$ cm^{-3} [5], $\Gamma_N = 1.5\times10^{-2}$, $n_e = 3.3$, $r_{41} = 1.4\times10^{-12}$ m/V, $R = 4.1\times10^{-19}$ m^2/V^2 [6], $E_B = 1\times10^7$ V/m, $\Gamma_{\mathrm{LEO}} = 0.6$ and $\Gamma_{\mathrm{QEO}} = 0.54$, we obtain $V_\pi = 0.5$V.

The parameters of the electrode can be calculated using the equivalent circuit shown in Fig. 3. Ignoring the very small R_p value, we obtain the phase velocity, v_{ph}, characteristic impedance, Z_0 and electrical attenuation coefficient, $\alpha(f)$ of the electrode as:

$$v_{\mathrm{ph}} = \sqrt{\frac{1}{L_u(C_u + 2\Delta C)}},$$

$$Z_0 = \sqrt{\frac{L_u}{C_u + 2\Delta C}}$$

$$\alpha(f) = \alpha_0(f)\sqrt{1 + \frac{2\Delta C}{C_u}}.$$

$\alpha_0(f)$ is the attenuation coefficient of the unloaded coplanar line, which can be calculated using existing empirical formulas [7]. $\Delta C = (k/d)C_{\mathrm{epi}}$, where C_{epi} is the capacitance of the epilayer or i region between the top and bottom ohmic contacts. Our prior work on similar electrodes verified these results [8]. Capacitive loading increases the capacitance per unit length of the electrode, which in turn decreases v_{ph} and Z_0. A decrease in the characteristic impedance increases attenuation coefficient due to increased current on the metal electrodes. For a traveling wave design maximizing bandwidth requires matching optical and microwave group velocities [9]. Furthermore, an electrode should not have any dispersion or its group and phase velocities should be the same. 3-dB bandwidth is reached at a frequency when electrode loss becomes 6.4 dB even when velocity matching is perfect [10]. For the reported device design, center conductor, gap and ground plane widths of the unloaded coplanar line are $W = 60$ μm, $g = 30$ μm, and $G = 150$ μm, respectively. Calculated unloaded line parameters are $L_u = 3.92$ nH/cm and $C_u = 0.89$ pF/cm. ΔC for contact widths $w1 = 2$ μm, $w2 = 2.5$ μm and fill factor of 0.6 is $\Delta C = 1.26$ pF/cm. These values give $v_{\mathrm{ph}} = 8.65$ cm/ns and $Z_C = 34$ Ω. Optical group velocity is calculated as 8.53 cm/ns. Hence velocity mismatch is less than 2%. The loss-limited 3-dB bandwidth for 1-μm-thick gold electrodes is 40 GHz.

Fabricated devices were cleaved and tested by end fire coupling in and out of the device using lensed fiber and a microscope objective, respectively. Measured transfer function of a 1-cm-long electrode device is shown in Fig. 4 both under single arm and push–pull drive conditions. Fits to data using the well-known Mach–Zehnder transfer function are also shown.

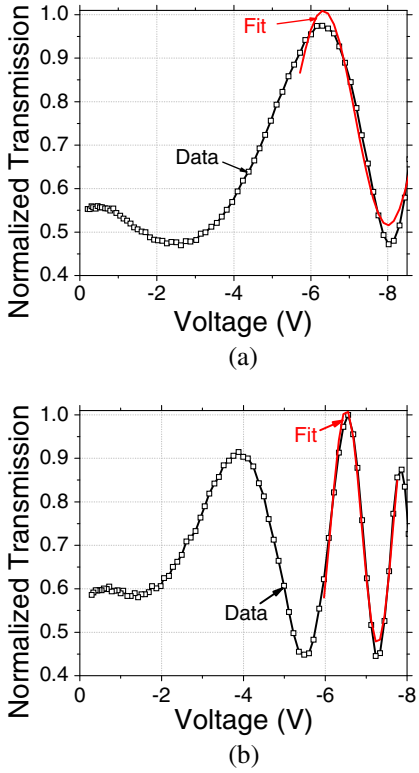

Fig. 4. (a) Transfer function of a 1-cm-long electrode device under single arm and (b) push–pull drive at 1.55 μm.

The extinction ratio shown in Fig. 4 is about 3 dB. This arises because it is not possible to couple all the incoming light into the semiconductor waveguide, and a significant amount of light also couples into the BCB layer used as the glue. This light is transmitted fairly efficiently due to large reflection resulting from high index contrast between the BCB and semiconductor epilayer/transfer substrate. Furthermore, this stray light is not modulated and remains in the output even if all the light through the modulator is turned off. In the measurements, it is very difficult to spatially filter this light, which provides a constant background level and degrades the extinction ratio. In an actual device, improving coupling efficiency using mode transformers or using a low index transfer substrate such as glass will improve the extinction ratio.

There is very little modulation up to about 4 V reverse bias. This is due to depletion of charge in the unintentionally doped i MQW and InP layers.

Once this charge depletes, a high electric field is set up on i layers and efficient modulation starts. Based on curve fitting, a V_π value of 1.6 V is obtained around 7 V bias and under single arm drive. This value reduces to 0.77 V around same bias under push–pull drive. Modulation becomes more efficient under increased reverse bias due to increased bias field. Increase bias field increases the effective LEO coefficient due to MQW, and modulation becomes more efficient. However, peak transmission also drops. This is due to quantum-confined stark effect (QCSE), which moves the tail of MQW absorption to longer wavelengths.

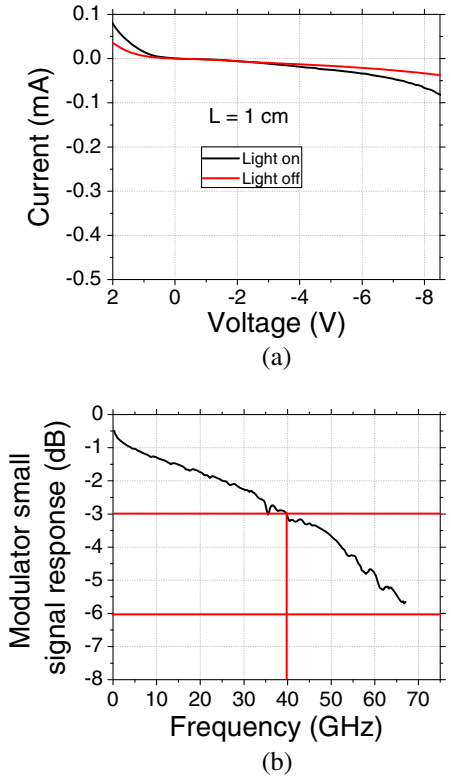

Fig. 5. (a) IV characteristics of a 1-cm-long electrode device with and without 1.55-μm radiation and (b) small signal modulation response of this device up to 67 GHz.

The effect of increased absorption is also evident in IV characteristics of the device shown in Fig. 5. Increase in reverse current under higher reverse bias when there is 1.55 μm radiation in the device is photo-detected current due to MQW absorption. This increases with increasing reverse bias due to QCSE. Around 7 V reverse bias, this current is less than 25 μA, and total reverse current is less than 50 μA. Measured small signal modulation response of this modulator under zero bias is shown in Fig. 5. 3-dB bandwidth corresponding to 3-dB reduction in electrical to electrical response is 40 GHz. 3-dB reduction in electrical to optical response, which corresponds to 6-dB reduction in this figure, is more than 67 GHz. This is the most commonly quoted bandwidth. Both measured V_π and bandwidth values are very close to the design targets.

We reported traveling wave electro-optic modulators with MQW cores in substrate removed waveguides. This design keeps optical propagation loss low by removing p doping from the waveguide and moving the PL absorption peak of the MQW core 180 nm away from the operating wavelength.

Furthermore large size of the waveguide makes coupling into the waveguide easier using simple mode transformers. Hence the total insertion loss can be kept low enough to make a practical device. Substrate removal allows placement of metal electrodes directly on both sides of the epilayer. This reduces ohmic losses significantly. Optical structure is broken into electrically isolated active modulator sections that periodically load a coplanar transmission line. This loading is mainly capacitive and increases the capacitance per unit length of the electrode. This is used for velocity matching to maximize the bandwidth. Presence of MQW core provides additional contribution to index change through QEO effect. Under drive conditions used, this contribution becomes very similar to LEO contribution with an effective LEO coefficient proportional to reverse bias field. Decrease in the QEO coefficient of the MQW due to increased detuning can be compensated using a larger bias field. Therefore, efficient modulation can be obtained. However, a large increase in the bias field also increases MQW absorption due to QCSE. Measurements at 7 V reverse bias and push–pull drive yield a V_π of 0.77 V for a modulator with 1-cm-long electrode and 60% fill factor. This corresponds to a modulation efficiency of 0.46 V cm, which is very close to the design value. 3 dB electrical to optical small signal modulation response of this device under zero bias is larger than 67 GHz. These values make the reported device the lowest drive voltage and widest bandwidth modulator ever fabricated.

References

1. K. Noguchi, O. Mitomi, and H. Miyazawa, J. Lightwave Technol. **16**, 615 (1998).
2. D. Chen, H. Fetterman, A. Chen, W. H. Steier, L. R. Dalton, W. Wang, and Y. Shi, Appl. Phys. Lett. **70**, 3335 (1997).
3. J. H. Shin, S. Wu, and N. Dagli, IEEE Photon. Technol. Lett. **19**, 1362 (2007).
4. S. Dogru and N. Dagli, J. Lightwave Technol. **LT-32**, 435 (2014).
5. B. R. Bennett, R. A. Soref, and J. A. Del Alamo, IEEE J. Quantum Electron. **26**, 113 (1990).
6. S. Dogru, J. H. Shin, and N. Dagli, *Proceedings of IEEE Photonics Society Annual Meeting*, Arlington, Va., October 9–13, 2011, pp. 739–740, Paper ThJ2.
7. G. E. Ponchak, M. Matloubian, and L. P. B. Katehi, IEEE Trans. Microwave Theor. Tech. **47**, 241 (1999).
8. J. H. Shin, S. R. Sakamoto, and N. Dagli, J. Lightwave Technol. **LT-29**, 48 (2011).
9. R. Spickermann, S. R. Sakamoto, and N. Dagli, *IEEE/LEOS 1996 Annual Meeting, Paper WM3*, Boston, Mass., November 18–21, 1996.
10. N. Dagli, IEEE Trans. Microwave Theor. Tech. **MTT-47**, 1151 (1999).